

How does vegetation affect sedimentation on tidal marshes? Investigating particle capture and hydrodynamic controls on biologically mediated sedimentation

Simon M. Mudd,¹ Andrea D'Alpaos,² and James T. Morris³

Received 14 October 2009; revised 23 March 2010; accepted 26 April 2010; published 28 August 2010.

[1] Plants are known to enhance sedimentation on intertidal marshes. It is unclear, however, if the dominant mechanism of enhanced sedimentation is direct organic sedimentation, particle capture by plant stems, or enhanced settling due to a reduction in turbulent kinetic energy within flows through the plant canopy. Here we combine several previously reported laboratory studies with an 18 year record of salt marsh macrophyte characteristics to quantify these mechanisms. In dense stands of *Spartina alterniflora* (with projected plant areas per unit volume of $>10 \text{ m}^{-1}$) and rapid flows ($>0.4 \text{ m s}^{-1}$), we find that the fraction of sedimentation from particle capture can instantaneously exceed 70%. In most marshes dominated by *Spartina alterniflora*, however, we find particle settling, rather than capture, will account for the majority of inorganic sedimentation. We examine a previously reported 2 mm yr^{-1} increase in accretion rate following a fertilization experiment in South Carolina. Prior studies at the site have ruled out organic sedimentation as the cause of this increased accretion. We apply our newly developed models of particle capture and effective settling velocity to the fertilized and control sites and find that virtually all ($>99\%$) of the increase in accretion rates can be attributed to enhanced settling brought about by reduced turbulent kinetic energy in the fertilized canopy. Our newly developed models of biologically mediated sedimentation are broadly applicable and can be applied to marshes where data relating biomass to stem diameter and projected plant area are available.

Citation: Mudd, S. M., A. D'Alpaos, and J. T. Morris (2010), How does vegetation affect sedimentation on tidal marshes? Investigating particle capture and hydrodynamic controls on biologically mediated sedimentation, *J. Geophys. Res.*, 115, F03029, doi:10.1029/2009JF001566.

1. Introduction

[2] Early studies of salt marsh development postulated that sedimentation rates decreased monotonically with increasing marsh elevation [e.g., Krone, 1987; French, 1993; Allen, 1994]. This stemmed from the observation that marshes lower in the tidal frame were inundated for longer periods of time resulting in greater particle settling during each tidal cycle. If the rate of sea level rise was to accelerate, increasing inundation would result in increased sedimentation and the marsh would eventually reach a depth in the tidal frame that allowed it to keep pace with this accelerated sea level rise. The only limit to accretion, under this paradigm, is the maximum accretion rate determined by the supply of sediment (i.e., the rate at which all sediment in suspension settles on the marsh platform during a tidal cycle). More recently, however, several authors have pro-

posed that salt marshes may drown even if the rate of sea level rise is less than the maximum accretion rate [e.g., Morris *et al.*, 2002; Marani *et al.*, 2007; Kirwan and Temmerman, 2009]. Crucial to these new predictions of marsh instability are the feedbacks between sedimentation, hydrodynamics, and the population dynamics of macrophytes living on the marsh surface.

[3] Numerous authors have noted that salt marsh macrophytes are most productive at an optimum elevation relative to sea level [e.g., Redfield, 1972; Orson *et al.*, 1985] and that they are restricted to a narrow range of elevations [e.g., Redfield, 1972; Orson *et al.*, 1985; Morris *et al.*, 2005]. It has also been established that salt marsh macrophytes play an important role in the capture and deposition of marsh sediments [e.g., Ranwell, 1964; Gleason *et al.*, 1979; Leonard and Luther, 1995; Neubauer, 2008; Li and Yang, 2009]. Morris *et al.* [2002] described a negative feedback between an increase in the rate of sea level rise and accretion on a salt marsh modulated by marsh vegetation. If the marsh elevation is lower than the optimum elevation, an increase in the depth of flooding during tides leads to a decrease in plant productivity and therefore a decrease in marsh accretion rates. In this unstable scenario, an increase in the rate of

¹School of GeoSciences, University of Edinburgh, Edinburgh, UK.

²Department of Geosciences, University of Padova, Padova, Italy.

³Belle W. Baruch Institute for Marine and Coastal Sciences, University of South Carolina, Columbia, South Carolina, USA.

sea level rise would lead to the drowning of the marsh: eventually, the marsh would become too deep for marsh macrophytes to survive. Indeed, both *Fagherazzi et al.* [2006] and *Marani et al.* [2007] identified this negative feedback as responsible for the bimodal distribution of elevations in typical estuaries. This bimodal distribution is due to the conversion of vegetated salt marshes to unvegetated mudflats. Because mudflats are less biologically productive than salt marshes and provide less protection from coastal storms, it is essential to acquire the ability to predict the critical rate of sea level rise at which this transition occurs.

[4] To predict how salt marshes will respond to changes in the rate of sea level rise, one must quantify the factors that control accretion rates on marshes. Marshes accrete through the settling of particles delivered to the marsh during tidally induced floods [e.g., *French and Stoddart*, 1992; *Christiansen et al.*, 2000], the direct capture of these particles by marsh macrophytes [e.g., *Stumpf*, 1983; *Leonard and Luther*, 1995], and direct deposition of organic matter due to root growth and litter deposition [*Nyman et al.*, 2006; *Neubauer*, 2008]. A detailed analysis of macrophyte growth characteristics combined with numerical modeling of marsh accretion that included direct deposition of organic sediment revealed that organic sedimentation can account for a substantial proportion of the accretion rate in slowly accreting marshes, but in rapidly accreting marshes mineral sediments must dominate [*Mudd et al.*, 2009]. This is because there are limits to marsh productivity and therefore organic sedimentation. In *Spartina alterniflora* marshes in South Carolina, the maximum organic production rate was estimated to be approximately $2 \text{ kg m}^{-2} \text{ yr}^{-1}$ [*Mudd et al.*, 2009]; this estimate was in line with other estimates of organic deposition on a wide variety of salt marshes [*Chmura et al.*, 2003]. If compressed organic matter has a density of 800 kg m^{-3} , even if the total production was to contribute to sediment accretion, we estimate that it would contribute a maximum of $\sim 2.5 \text{ mm yr}^{-1}$ to marsh accretion. Inorganic sedimentation must therefore be responsible for any accretion beyond this maximum organic rate.

[5] Because vegetation has been demonstrated to be critical in determining if a coastal area is composed of mudflats or salt marshes [*Fagherazzi et al.*, 2006; *Marani et al.*, 2007], it is essential to understand how vegetation affects sedimentation rates. A number of prior studies have adopted an approach in which sedimentation rates are assumed to be linearly proportional to the standing biomass on the marsh [e.g., *Gleason et al.*, 1979; *Morris et al.*, 2002; *Mudd et al.*, 2004; *D'Alpaos et al.*, 2007; *Kirwan and Murray*, 2007]. A recent laboratory study, however, has demonstrated that the rate stems can directly capture sediment (that is, the rate sediment is deposited directly on the plant surface and is nonlinearly related to flow velocity, particle diameter, and the physical characteristics of plants exposed to tidally induced flood waters) [*Palmer et al.*, 2004]. By combining the laboratory results of *Palmer et al.* [2004] and work by *Mudd et al.* [2004] that quantified the relationship between standing biomass and other physical characteristics of marsh plants such as stem density and diameter, *D'Alpaos et al.* [2006] were able to quantify particle capture rates as a function of biomass on vegetated marsh surfaces. Plants are also expected to influence accretion rates not only through

direct capture but also by reducing turbulent energy within the marsh canopy [e.g., *Leonard and Croft*, 2006], which can in turn affect effective settling velocities of particles suspended in tidally induced flood waters [e.g., *Leonard and Luther*, 1995; *Nepf*, 1999].

[6] In this study, we report an expanded data set quantifying the relationship between the physical characteristics of salt marsh macrophytes as a function of biomass for several *Spartina alterniflora* marshes in South Carolina, USA. These data are compared with characteristics from different plant species and locations reported in the literature and used to quantify the predicted accretion rate of sediment due to capture on typical salt marshes using the laboratory based model of *Palmer et al.* [2004]. We also develop a model that quantifies changes in the effective settling velocity of particles by combining our measured macrophyte characteristics with the laboratory results of *Nepf* [1999] relating turbulent kinetic energy to drag forces and *Tanino and Nepf* [2008] relating drag forces to the physical characteristics of emergent vegetation. Using these two newly developed models, we then examine the increase in accretion following a fertilization experiment reported by *Morris et al.* [2002] in order to understand if this increase is better explained by enhanced settling caused by a reduction of turbulent energy through the denser fertilized vegetation or by enhanced particle capture. Thus, we aim to advance our understanding of marsh accretion processes and how they relate to salt marsh macrophytes in order to improve our ability to predict the stability and longevity of coastal salt marshes.

2. Accretion on Marsh Platforms

[7] At any given point on a marsh, the rate of change in marsh surface elevation can be described by

$$\frac{\partial \zeta_s}{\partial t} = Q_c / \rho_s + Q_s / \rho_s + O - E - \text{Cmp}, \quad (1)$$

where ζ_s [dimension L; dimensions of variables in [L]length [M]mass and [T]time henceforth listed in square brackets] is the elevation of the marsh surface, ρ_s [M L^{-3}] is the density of the marsh sediments, Q_c [$\text{M L}^{-2} \text{ T}^{-1}$] is the rate of mass captured directly by plants stems per unit area of the marsh, Q_s [$\text{M L}^{-2} \text{ T}^{-1}$] is the rate of mass that settles out of suspension onto the surface of the marsh, O [L T^{-1}] is an organic accretion rate, E [L T^{-1}] is the erosion rate, and Cmp [L T^{-1}] is the rate of compaction. The majority of both distributed [*Mudd et al.*, 2004; *Temmerman et al.*, 2005; *D'Alpaos et al.*, 2007; *Kirwan and Murray*, 2007] and zero-dimensional [e.g., *French*, 1993] models of marsh evolution neglect compaction [c.f., *Mudd et al.*, 2009] and typically use empirical rather than physically based equations to quantify Q_c and Q_s [e.g., *Morris et al.*, 2002]. Here by assimilating prior laboratory-based results with our own field measurements, we attempt to better constrain both Q_c and Q_s .

3. Model of Particle Capture Rates as a Function of Biomass on Vegetated Salt Marshes

[8] *Palmer et al.* [2004] idealized particle capture by salt marsh macrophytes as the capture of particles by cylindrical structures in low Reynolds number flow. We follow their

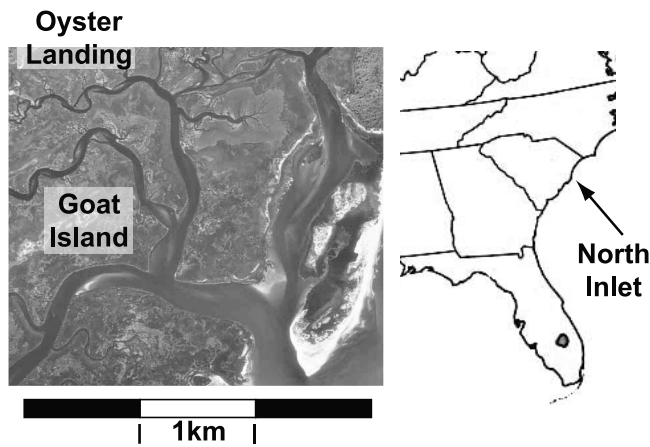


Figure 1. Location map and aerial photograph of the study sites in the North Inlet estuary, South Carolina, USA.

approach and consider the particle capture rate of sediment on salt marsh macrophytes during tidally induced floods to be proportional to both the flux of particles past marsh

macrophytes and the area upon which particles can be trapped. This can be described as

$$\frac{\partial P}{\partial t} = \frac{\eta P u d_c l_c}{V}, \tag{2}$$

where P is the number of particles per unit volume of water, η is a dimensionless particle capture efficiency, u [$L T^{-1}$] is the flow velocity, d_c [L] is the diameter of the collector (the stem diameter), l_c [L] is the total length of the collector (i.e., the total length of stems within a control volume), and V [L^3] is the volume of water flowing through the marsh macrophytes. The total length of collector is equal to the number of stems times the length of stems exposed to water; in emergent vegetation, this length is the flow depth. The volume of water per unit area is the flow depth, so therefore,

$$\frac{l_c}{V} = n_c, \tag{3}$$

where n_c is the number of stems per unit area. Noting that the concentration (C [$M L^{-3}$]) of particles in the water is

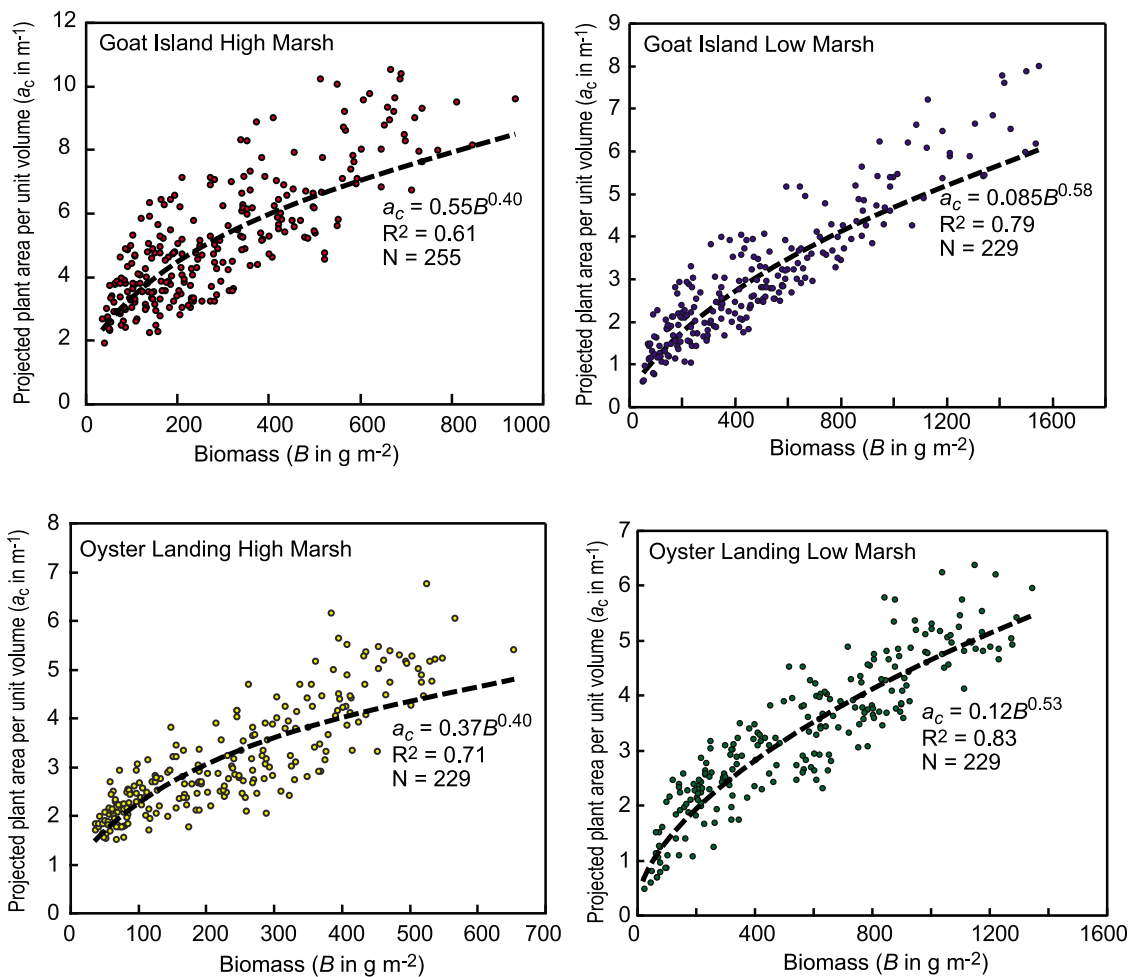


Figure 2. The projected plant area per unit volume as a function of biomass for four sites at North Inlet. Measurements of individual plant heights and masses were taken monthly for approximately 18 years. Data in this plot were calculated based on these direct measurements and a previously reported relationship between plant mass and projected area [Morris, 1989].

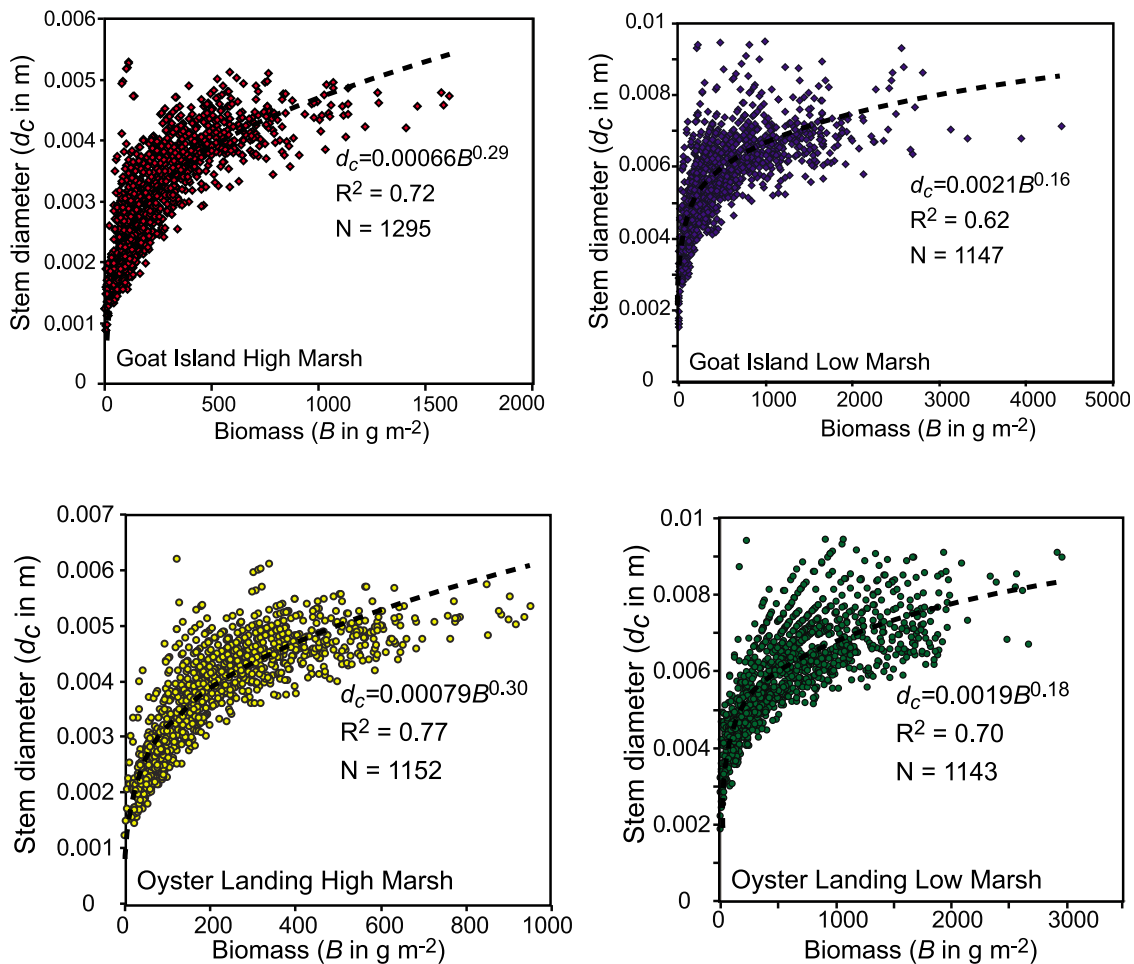


Figure 3. The mean stem diameter as a function of biomass for four sites at North Inlet. Each site had six control plots, measured monthly for approximately 18 years. Direct measurements were taken of biomass, stem height, and stem density [e.g., *Morris and Haskin*, 1990]; the data in this plot were calculated based on direct measurements.

equal to the number of particles per unit volume of water times the mass per particle, we find that

$$Q_c = \eta C u d_c n_c h, \quad (4)$$

where h [L] is the flow depth. Using a series of laboratory experiments, *Palmer et al.* [2004] found the particle capture efficiency to be

$$\eta = \kappa (Re_c)^\gamma (R)^\sigma, \quad (5)$$

where Re_c [dimensionless] is the Reynolds number based on the collector diameter ($Re_c = u d_c / \nu$ where ν [$L^2 T^{-1}$] is the kinematic viscosity of water), R [dimensionless] is the ratio of particle diameter to collector diameter ($R = d_p / d_c$ where d_p [L] is the particle diameter), and κ , γ , and σ [dimensionless] are empirical coefficients. To estimate sedimentation rates based on particle capture, the physical attributes of the marsh vegetation must be quantified. On the basis of a long-term record of marsh productivity [*Morris and Haskin*, 1990], *Mudd et al.* [2004] found that the projected plant area per unit volume (a_c , dimensions L^{-1})

and stem diameter d_c could be described as a power law function of biomass,

$$a_c = \alpha B^\beta, \quad (6)$$

$$d_c = \mu B^\phi, \quad (7)$$

where B [$M L^{-2}$] is the biomass per unit area of marsh macrophytes and α , β , μ , and ϕ are empirical coefficients. The projected plant area per unit volume is simply the total area of plant material projected orthogonal to the flow direction within a $1 m^3$ volume [*Nepf*, 1999]. In an array of cylinders, a_c can be computed with $a_c = d_c n_c$ [e.g., *Nepf*, 1999]; here we use direct measurements of stem densities and leaf areas to calculate a_c . Combining equations (4)–(7) and multiplying both sides of the resulting equation by the mass per sediment particle, we find that

$$Q_c = \frac{\alpha \kappa}{\nu^\gamma} \mu^{\gamma-\sigma} C h u^{1+\gamma} B^{\beta+\phi(\gamma-\sigma)} d_p^\sigma. \quad (8)$$

[9] To parameterize equations (6) and (7), *Mudd et al.* [2004] used monthly measurements of stem densities and

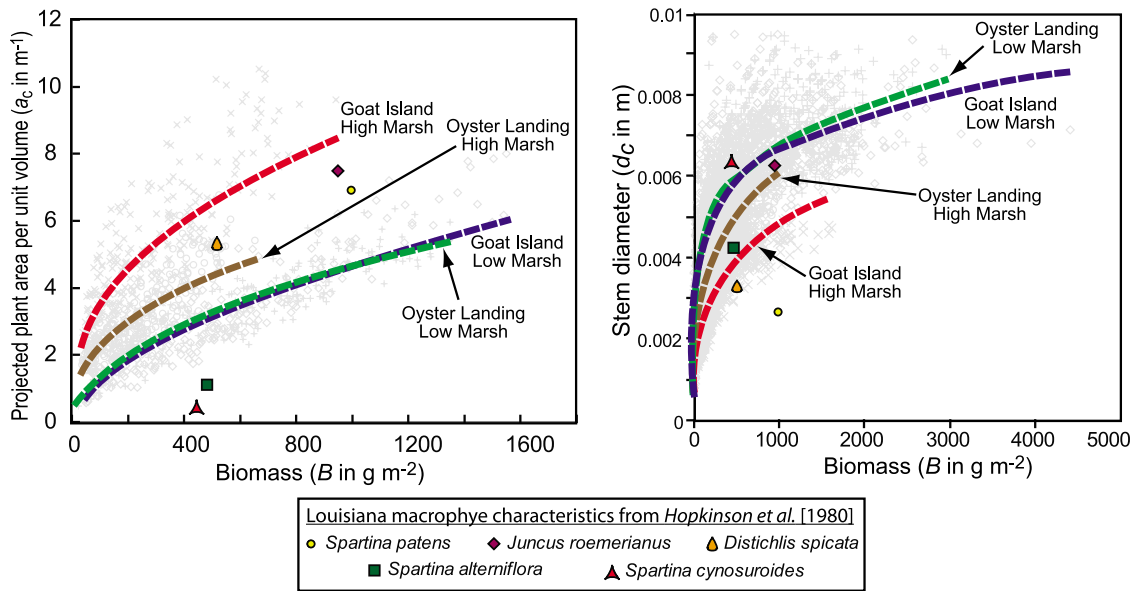


Figure 4. Comparison of North Inlet data with the data from Louisiana from *Hopkinson et al.* [1980]. *Hopkinson et al.* [1980] report average annual biomass, stem density, average mass per stem, and a regression equation relating stem mass to stem height. The data in this plot were calculated based on that regression and assuming the dry bulk density of plant material was 150 kg m^{-3} .

standing biomass and combined these with relationships between stem height and biomass reported by *Morris and Haskin* [1990]. Specifically, measured biomass was divided by stem density to give a mean weight per stem. This was converted to volume per stem using the measured average dry bulk density of *Spartina* stems (150 kg m^{-3} , $N = 30$, standard deviation 38 kg m^{-3}) and diameter was then calculated by combining the volume per stem with measured stem heights [*Morris and Haskin*, 1990]. These data were used to calculate the projected plant area per unit volume and stem diameter for a single plot, dominated by *Spartina alterniflora*, at North Inlet, South Carolina. Here we present calculations of the projected plant area per unit volume and stem diameter for 18 years of monthly measurements from 24 plots on both high and low *Spartina alterniflora*-dominated marshes at two locations in North Inlet (Figure 1). This expanded data set shows the natural variability of the projected stem area per unit volume and stem diameter for a single estuary (Figures 2 and 3).

[10] Parameter values for the Goat Island high marsh are slightly different from those reported by *Mudd et al.* [2004]. *Mudd et al.* [2004] calculated projected areas and stem diameters based on plant heights as calculated by *Morris and Haskin* [1990]. Here we use measurements of individual plant masses that are combined with a regression of plant mass to leaf area from *Morris* [1989], stem density and stem diameter to form a more accurate data set than that calculated by *Mudd et al.* [2004].

[11] The data set for projected area (Figure 2) is smaller than the data set of calculated diameters (Figure 3), because monthly measurements of the mass of every plant in a plot were only carried out on a subset of the experimental plots whereas stem diameters were calculated by combining the larger data set of biomass and stem density with relationships between biomass and plant heights (see text following equation (8)). These data are appropriate for vegetation that

remains emergent at high tide but inappropriate when high water submerges the canopy. Indeed, some of the marsh plants are shorter than the inundation depth at mean high tide ($\sim 40 \text{ cm}$ at low marsh sites and $\sim 10 \text{ cm}$ at high marsh sites). Because equation (4) multiplies the projected area per unit volume by the flow depth, but some stems do not interact with the entire flow depth, the regressions presented here should be considered maximum estimates of projected area per unit volume. We use these maximum estimates of projected area per unit volume to calculate the maximum rate at which sediment accretes on the marsh due to particle capture. As we demonstrate later in this contribution, the flow conditions at North Inlet are such that particle capture can only represent a small ($<5\%$) contribution to the total rate of sedimentation on the marsh; in this setting, a complete reconstruction of the canopy structure is unnecessary. However, in marshes with flow conditions more amenable to particle capture by marsh vegetation (i.e., marshes with faster flow or coarser sediment; see below), a more complete analysis of the canopy structure may be necessary because capture is more prevalent near the marsh surface [e.g., *Li and Yang*, 2009] and our averaging approach will overestimate capture during the highest tides.

[12] While the 18 year record of allometric measurements of marsh macrophytes at North Inlet is unique, some measurements, albeit less comprehensive, are available from other marshes for comparison. *Hopkinson et al.* [1980] reported average annual macrophyte characteristics for several species in a Louisiana salt marsh. On the basis of their data (and assuming a dry bulk density of plant stems of 150 kg m^{-3} ; this is the bulk density of *Spartina alterniflora* measured at North Inlet) we have calculated mean annual stem diameter and projected stem area per unit volume for several species of marsh macrophytes in the Louisiana marsh studied by *Hopkinson et al.* [1980]. These data are plotted with the range of values obtained from North Inlet (Figure 4).

Data for *Sagittaria falcata* reported by *Hopkinson et al.* [1980] are excluded from our analysis because it has broad leaves compared to the other species and therefore does not conform to the assumptions of the *Palmer et al.* [2004] model.

[13] Both stem diameters and projected plant areas in the Louisiana marshes studied by *Hopkinson et al.* [1980] are similar to those at North Inlet (Figure 4b). *Pezeshki and DeLaune* [1988] reported projected plant areas for *Spartina alterniflora* on Louisiana marshes that are consistent with the measurements of *Hopkinson et al.* [1980]. On the basis of the reported data of *Pezeshki and DeLaune* [1988], we calculate that the projected area per unit volume of *Spartina alterniflora* ranges from ~ 0.4 to 2.7 m^{-1} for biomass of ~ 600 – 2000 g m^{-2} on high marshes and from ~ 1.1 to 4.6 m^{-1} for biomass of 1400 – 2800 g m^{-2} on low marshes in Louisiana. These data are based on monthly measurements taken from March to October in 1 year; they are insufficient to create regressions similar to those in Figures 2 and 3. These data suggest, however, that projected areas per unit volume are similar to or slightly lower in Louisiana marshes compared to those at North Inlet.

[14] Other authors have reported stem diameters and stem densities for higher latitude marshes. *Valiela et al.* [1978] reported stem densities between 233 and 400 stems per square meter and average stem diameters between 2 and 5 mm for seven plots of *Spartina alterniflora* at the Great Sippewissett Marsh in Massachusetts. On the basis of *Valiela et al.*'s [1978] data the projected plant area per unit volume of these sites ranged from ~ 1.2 to 2.6 m^{-1} . *Lightbody and Nepf* [2006] reported stem diameters of 1.7 mm at 10 cm above the marsh surface in a *Spartina alterniflora* marsh at the Plum Island estuary in Massachusetts and directly measured the projected plant area per unit volume, which peaked at $\sim 6.7 \text{ m}^{-1}$ at 11 cm from the marsh surface and declined rapidly with increasing height.

[15] Because North Inlet marshes have high productivity relative to marshes at higher latitudes [e.g., *Kirwan et al.*, 2009], similar stem densities and greater stem diameters compared to microtidal marshes on the gulf coast [e.g., *Hopkinson et al.*, 1980; *Leonard and Luther*, 1995], and similar or greater estimated projected plant areas per unit volume than marshes on the Gulf and north-east coasts of the United States [*Valiela et al.*, 1978; *Hopkinson et al.*, 1980; *Lightbody and Nepf*, 2006], we consider North Inlet marshes to have a relatively high potential for sedimentation due to particle capture compared to other marshes where data are available.

4. Marsh Vegetation and Enhanced Particle Settling

[16] To compare accretion rates due to settling and particle capture, we must quantify settling rates on the marsh surface. The instantaneous settling rate of the particles is

$$Q_s = w_{\text{eff}} C, \quad (9)$$

where w_{eff} [L T^{-1}] is the effective settling velocity of the particles in suspension. Below we calculate particle concentrations as they evolve during tidally induced flooding, but first we examine instantaneous settling and particle capture rates for fixed sediment concentrations.

[17] Turbulence can affect effective settling velocities of particles, and reductions in turbulent energy can lead to enhanced particle settling in the marsh setting [e.g., *Leonard and Luther*, 1995; *Nepf*, 1999; *Christiansen et al.*, 2000; *Leonard and Croft*, 2006]. We define the effective settling velocity (w_{eff}) as the settling velocity in turbulence-free water (w_s) minus any component of upward motion caused by turbulence (w_{up}). The settling velocity of particles in turbulence-free water depends on the particles' shape and size [e.g., *Dietrich*, 1982]. *Camenen* [2007] examined data from five decades of experimental studies and found that settling velocity could be described as

$$w_s = \frac{\nu}{d_p} \left[\sqrt{\frac{1}{4} \left(\frac{A}{F}\right)^{2/m} + \left(\frac{4d_p^3 g[s-1]}{3F\nu^2}\right)^{1/m}} - \frac{1}{2} \left(\frac{A}{F}\right)^{1/m} \right]^m, \quad (10)$$

where A , F , and m are dimensionless coefficients that depend on the material and shape of the particle, g [L T^{-2}] is the acceleration due to gravity, and s [dimensionless] is the ratio between the particle density and the density of water.

[18] According to the Rouse equation [e.g., *Christiansen et al.*, 2000; *Orton and Kineke*, 2001], the upward velocity of sediment particles is equal to

$$w_{\text{up}} = \kappa_{\text{vk}} u_*, \quad (11)$$

where κ_{vk} is von Karman's constant, assumed to be 0.4, and u_* [dimensions L T^{-1}] is the shear velocity. The shear velocity is

$$u_* = \sqrt{\frac{\tau}{\rho_w}}, \quad (12)$$

where τ [$\text{M L}^{-1} \text{ T}^{-1}$] is the shear stress and ρ_w [M L^{-3}] is the density of water. Several authors have found that shear stress is correlated to total kinetic energy,

$$\tau = \omega k, \quad (13)$$

where ω is a constant of proportionality and k [$\text{L}^2 \text{ T}^{-2}$] is the turbulent energy per unit mass of water. The shear stress that results in $w_{\text{up}} = w_s$ is equivalent to the critical shear stress that other authors use as an erosion threshold on marsh surfaces [e.g., *D'Alpaos et al.*, 2007; *Kirwan and Murray*, 2007]. *Kim et al.* [2000] found $\omega = 0.21$, *Soulsby and Dyer* [1981] found $\omega = 0.20$, and *Stapleton and Huntley* [1995] found $\omega = 0.19$. So we find shear velocity is

$$u_* = \sqrt{\frac{0.20k}{\rho_w}}. \quad (14)$$

[19] *Nepf* [1999] reported that turbulent energy per unit mass of water k in an array of emergent cylinders could be described as

$$k = \alpha_k^2 u^2 (C_D a d_c)^{2/3}, \quad (15)$$

where α_k is a coefficient reported to be 0.9 by *Nepf* [1999] and C_D is the depth averaged drag coefficient within the array of cylinders. *Tanino and Nepf* [2008] reported that the

drag coefficient in an array of emergent cylinders can be described as

$$C_D = 2 \left(\frac{\alpha_0}{Re_c} + \alpha_1 \right). \quad (16)$$

[20] *Tanino and Nepf* [2008] report that α_1 is a function of the solid fraction of the cylinders within the flow. The solid fraction is the area of a single cylinder in cross section times the number of cylinders per unit volume or $\pi ad_c/4$. Although *Tanino and Nepf* [2008] argue that the parameter α_0 should also be a function of the solid fraction, the evidence for a relationship between α_0 and the solid fraction is sparse; we assume it is a constant at the low solid fractions typically present on marsh surfaces. By combining equations (6), (7), and (16), we find that the drag coefficient can be quantified as a function of biomass and flow velocity,

$$C_D = 2 \left(\frac{\alpha_0 v}{u \mu B^\phi} + \chi + \zeta \frac{\alpha \mu \pi}{4} B^{\beta+\phi} \right), \quad (17)$$

where χ and ζ are empirical coefficients reported by *Tanino and Nepf* [2008] to be 0.46 ± 0.11 and 3.8 ± 0.5 , respectively. On the basis of the force balance of water at low Reynolds number, the water surface slope S required to generate a flow velocity through a particular stand of vegetation can be determined by

$$\frac{C_D u^2}{2} a = - \left(1 - \frac{\pi ad}{4} \right) S. \quad (18)$$

[21] Equations (15) and (17) can be combined to calculate the turbulent kinetic energy for a given biomass, and this information, combined with equations (10) and (11), can be used to calculate the effective settling velocity as a function of flow velocity, biomass, and particle diameter. Flocculation can also affect particle settling velocities, but *Christiansen et al.* [2000] found that most sediments settling in the high marsh setting are not flocculated; for simplicity, we assume flocculation does not significantly affect effective settling velocities.

5. A Combined Analysis of Trapping and Settling on Marsh Surfaces

[22] Equations (9)–(18) allow prediction of capture and trapping based on local flow conditions and vegetation characteristics. These can be used in either distributed or zero-dimensional (e.g., a point on the marsh surface) models of marsh evolution, although in a zero-dimensional model the resulting sedimentation rates should be considered representative of only local conditions and not generally of the entire marsh because particle concentrations, flow velocities, and flow depths vary as function of distance from tidal channels [e.g., *Leonard and Luther*, 1995; *Christiansen et al.*, 2000; *Neumeier and Ciavola*, 2004; *Yang et al.*, 2008].

[23] Using equations (8)–(18), we are able to quantify the fraction of sediment flux from tidal flood waters due to particle capture (i.e., $Q_c/Q_T = Q_c/(Q_c + Q_s)$ where Q_T is the total sedimentation rate due to both settling and particle capture; direct organic sedimentation is excluded. Examination of these equations reveals that the fraction of sedimentation due to particle capture is not a function of particle

concentration, although the total sedimentation rate due to settling and particle capture is linearly dependent on sediment concentration in tidal flood waters.

[24] The fraction of sedimentation due to particle capture, Q_c/Q_T , is linearly proportional to flow depth h less than linearly related to biomass but is strongly nonlinearly related to particle diameter and flow velocity. Both the trapping flux (equation (8)) and the settling flux (equations (9)–(18)) are nonlinear functions of flow velocity and particle diameter. A small increase in flow velocity will lead to a large increase in the fraction of sedimentation due to particle capture.

[25] A contour plot of the ratio $Q_c/Q_T = Q_c/(Q_c + Q_s)$ is shown in Figure 5 for Goat Island High Marsh (the site with plants most efficient at particle capture) and Oyster Landing Low Marsh (the site with plants the least efficient at particle capture). Parameter values are shown in Table 1. In Figure 5 the ratio Q_c/Q_T is calculated instantaneously (e.g., not averaged over a year; we investigate longer-term sedimentation in the flowing sections) for a given particle size, flow velocity, flow depth, and biomass. Because the ratio Q_c/Q_T is not a function of particle concentration, the relative contribution trapping and settling fluxes will not be affected if one process preferentially removes sediment from the water column so the two processes are decoupled on a short time scale. They are only coupled on a longer time scale if enhanced settling from one mechanisms changes the elevation of the marsh, which in turn affects standing biomass [e.g., *Morris et al.*, 2002], altering both trapping efficiency and drag on the marsh. We examine this effect in section 6.

[26] The range of particle sizes, flow velocities, and flow depths used to generate Figure 5 are based on measured values. Particle sizes in estuarine environments reported in the literature range from clays to sands, with mean grain sizes in the silt to fine sand ranges 4–250 μm [e.g., *Bradley and Morris*, 1990; *Shimeta and Jumars*, 1991; *Netto and Lana*, 1997; *Amos et al.*, 2004]. Typical velocities range from nil at slack water to 0.4 m s^{-1} in a wide range of marsh environments, with most reported velocities being $<0.1 \text{ m s}^{-1}$ [e.g., *Leonard and Luther*, 1995; *Yang*, 1998; *Shi et al.*, 2000; *Neumeier and Ciavola*, 2004; *Temmerman et al.*, 2005; *Leonard and Croft*, 2006; *Torres and Styles*, 2007]. *Torres and Styles* [2007] found that velocities were generally less than 0.1 m s^{-1} on the marsh platform at North Inlet and typically in the range of 0.05 m s^{-1} . For silt particles on Goat Island high marsh during a flood with a velocity of 0.05 m s^{-1} , 0.1 m deep flood waters (the typical flooding depth on Goat Island high marsh) and biomass of 280 g m^{-2} (the mean annual biomass on Goat Island High Marsh), approximately 1.7% of the sediment delivered from flood waters is retained on the marsh due to particle capture. The Goat Island high marsh sites are located between 45 and 50 cm above mean sea level; the tidal range at North Inlet is ~ 1.4 m. Interannual variability in mean high tide approaches 20 cm [*Morris et al.*, 2002]. During abnormally high floods (flow depth = 0.35 m) when biomass is at its peak (780 g m^{-2}), particle capture may reach 39% of the total inorganic sedimentation. Such circumstances, however, are rare.

[27] The fraction of sediment flux from tidal flood waters due to particle capture is plotted as a function of biomass for all four sites in Figure 6. For low marsh sites, as well as a fertilized site on Goat Island, increasing biomass leads to

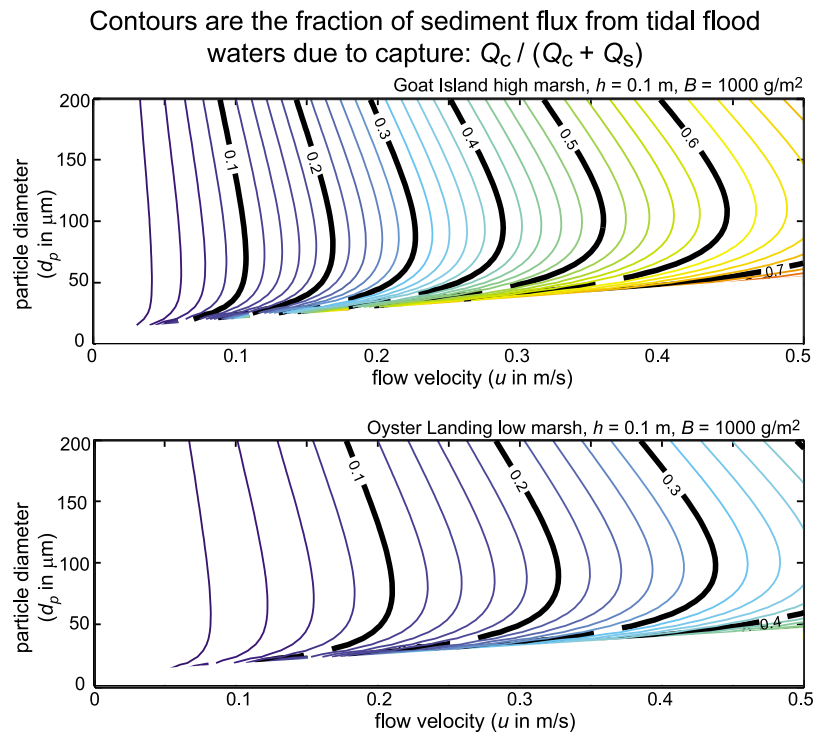


Figure 5. Contour plots of the fraction $Q_c/Q_T = Q_c/(Q_c + Q_s)$, which is the fraction of total sediment flux from tidal flood waters due to particle capture. Contour plots are of instantaneous sedimentation ratio (i.e., not integrated over a tidal cycle).

increased particle capture efficiency (Figure 6). *Li and Yang* [2009] also found a positive relationship between biomass and particle capture on a sediment rich, mesotidal low marshes near Shanghai populated by *Spartina alterniflora*. The high marsh sites at North Inlet (three sites at Goat Island and three sites at Oyster Landing), in contrast, have annually

averaged capture efficiencies that are negligibly or even inversely related to biomass. In these marshes increases in biomass do not lead to similar increases in sedimentation due to particle capture because the peak biomass and peak stem densities are out of phase [e.g., *Morris and Haskin*, 1990]: peak biomass does not occur at the same time as peak stem density. On Oyster Landing high marsh, where increases in biomass lead to decreases in particle capture

Table 1. Parameter Values Used in Particle Capture Calculations^a

Parameter	Value	Reference or Notes
κ	0.224	<i>Palmer et al.</i> [2004]
γ	0.718	<i>Palmer et al.</i> [2004]
σ	2.08	<i>Palmer et al.</i> [2004]
α	0.085–0.55	This study (Figure 2)
β	0.40–0.58	This study (Figure 2)
μ	0.00066–0.0021	This study (Figure 3)
ϕ	0.16–0.30	This study (Figure 3)
A	38.0	<i>Camenen</i> [2007] for silt
F	3.55	<i>Camenen</i> [2007] for silt
M	1.12	<i>Camenen</i> [2007] for silt
α_k	0.9	<i>Nepf</i> [1999]
χ	0.46	<i>Tanino and Nepf</i> [2008]
ζ	3.8	<i>Tanino and Nepf</i> [2008]
α_0	11	<i>Tanino and Nepf</i> [2008]
ν	10^{-6} m ² s ⁻¹	Water at 20°C
κ_{vk}	0.4	Von Karman constant
ω	0.2	<i>Soulsby and Dyer</i> [1981]
s	2.65	On the basis of typical density of silicate minerals
ρ_s	800 kg m ⁻³	For Goat Island, <i>Bradley and Morris</i> [1990]

^aThe values of parameters α and σ are reported such that equation (5) returns the projected plant area per unit volume in the units m⁻¹ if biomass is in units g m⁻². The values of parameters μ and ϕ are reported such that equation (6) returns the stem diameter in the units of m if biomass is in units g m⁻². All other parameters are dimensionless unless otherwise noted.

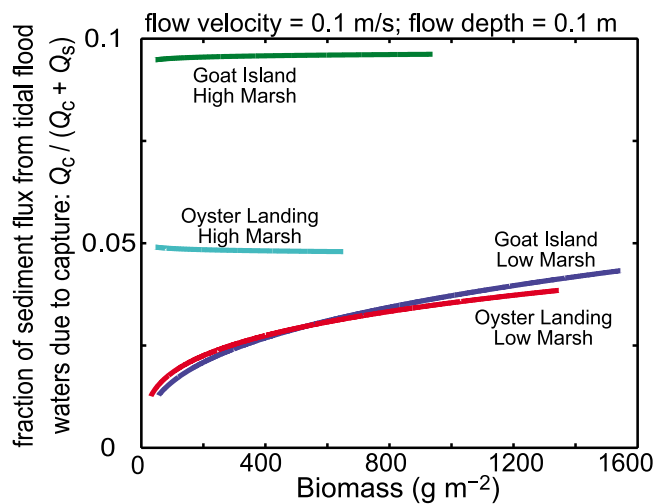


Figure 6. The fraction of sediment flux from tidal flood waters due to particle capture as a function of biomass for all four sites at North Inlet, South Carolina, USA. Range of biomass for each site is the same as in Figure 2. Particle diameter is 40 μ m.

efficiency, stem densities during periods of peak biomass are sufficiently low to reduce particle capture at peak biomass, despite the greater projected area of individual plants.

[28] It should be noted that equation (8) is only valid for flow depths less than the canopy height, so early in the growing season when stems are short the sedimentation due to particle capture will be less than that predicted in Figure 6. However, marsh platforms typically occur near the elevation of high tide [e.g., *Krone*, 1987] and many coastal marshes, particularly high marshes, are either emergent throughout the tidal cycle or emergent with only the exception of the highest (i.e., spring) tides [e.g., *Leonard and Luther*, 1995; *Morris et al.*, 2002; *Lightbody and Nepf*, 2006; *Yang et al.*, 2008].

6. Factors Controlling the Observed Increase in Accretion due to Fertilization at North Inlet

[29] *Morris et al.* [2002] reported that marsh accretion rates at a fertilized site within the Goat Island high marsh were 7.1 mm yr^{-1} between 1997 and 2000; this is in contrast to an accretion rate of 5.1 mm yr^{-1} at a nearby, unfertilized control plot. Although mean aboveground dry matter production increased from $780 \pm 50 \text{ g m}^{-2}$ in a control plot to $3280 \pm 300 \text{ g m}^{-2}$ in the fertilized plots (years 1987–1996) [*Morris and Bradley*, 1999], the increased accretion could not be explained by direct organogenic deposition of biomass in the top 5 cm of sediment: *Morris and Bradley* [1999] found that fertilized sites had lower organic matter content in the top 5 cm of sediment and speculated that this was caused by dilution due to increased inorganic sedimentation. Marker horizon data reported by *Morris et al.* [2002] confirmed that the increase in accretion was due to the enhanced accumulation of sediment deposited on the marsh surface. Here we aim to understand if this increased accretion rate can be explained solely by increased particle capture or is instead due to a combination of changes in particle capture and hydrodynamics that occur as a result of increased biomass. To do this, we examine the sensitivity of particle capture and settling as a function of both particle size and flow velocity over the range of these values measured at nearby sites to ascertain if either enhanced capture or settling can explain the increase in accretion measured on the fertilized sites.

[30] To estimate sediment flux rates, we integrate equations (8)–(18) over a tidal cycle. North Inlet has a semidiurnal tidal cycle [*Morris et al.*, 2002] and tidal range of 1.4 m. The equations are integrated for two tidal cycles daily over 1 year; biomass is assumed to vary sinusoidally as a function of the Julian day, with peak biomass occurring during the summer [e.g., *Mudd et al.*, 2004, 2009]. Minimum and maximum standing biomass values from fertilized and unfertilized plots were calculated based on the average February standing biomass and average August and September standing biomass for the years 1997–2000 (the years for which *Morris et al.* [2002] report accretion rates). Minimum and maximum biomass on the fertilized plots was 760 and 2170 g m^{-2} , respectively. Minimum and maximum biomass on the unfertilized plots was 120 and 540 g m^{-2} , respectively. The control and fertilized plots occur at $\sim 15 \text{ cm}$ below mean high tide, but interannual variability in mean high tide approaches 20 cm [*Morris et al.*, 2002], so we consider, as two end-member scenarios, flow depths at high tide of

5 and 35 cm. While we do not have direct measurements of flow velocities and suspended sediment concentrations at the site, we can make estimates of their values based on nearby measurements. *Torres and Styles* [2007] recorded flow velocities of up to 10 cm s^{-1} on the marsh surface. We vary velocity sinusoidally from 0 to 10 cm s^{-1} with the minimum velocity occurring at slack water and the maximum occurring as the tidally forced water level is rising at its fastest rate during the tidal cycle. *Bradley and Morris* [1990] report a bulk density of 800 kg m^{-3} at a nearby site. Mean particle sizes on Goat Island range from fine sand ($\sim 64 \mu\text{m}$) to medium silt ($\sim 20 \mu\text{m}$) [*Bradley and Morris*, 1990; *Gardner and Porter*, 2001]. *Gardner and Porter* [2001] concluded, based on radiocarbon dating of buried organic fragments that the majority of the sands found at North Inlet were Pleistocene in age, and modern sand deposits were locally reworked Pleistocene sands. Sediments currently being deposited by tidally induced floods on Goat Island are predominantly composed of medium silt [*Gardner and Porter*, 2001]. In our simulations, we consider both medium silt of $20 \mu\text{m}$ and coarse silt of $60 \mu\text{m}$ as end-members. Suspended sediment concentrations have not been measured on the marsh platform; instead we calibrate suspended sediment concentrations in order to match the accretion rates measured by *Morris et al.* [2002]. For context, *Gardner et al.* [2006] measured sediment concentrations of $\sim 28 \text{ mg L}^{-1}$ in nearby tidal creeks. Other parameter values are listed in Table 1.

[31] During the rising limb of the tide, we make the simplification that sediment concentrations are fixed due to a supply of sediment-laden water from tidal creeks. On the falling limb sediment is no longer supplied from tidal creeks and suspended sediment concentrations fall as sediment settles or is captured. Thus, we solve the sediment concentration by integrating the continuity equation [*Krone*, 1987; *Temmerman et al.*, 2003; *Marani et al.*, 2007],

$$\frac{\partial C}{\partial t} = -\frac{Q_c}{h} - \frac{Q_s}{h} - \frac{C}{h} \frac{\partial h}{\partial t}. \quad (19)$$

[32] Calibrated values of suspended sediment concentration for medium silt are 29.9 mg L^{-1} if flow depths are 5 cm during high tide and 19.5 mg L^{-1} if flow depths are 35 cm during high tide. Capture accounts for 0.35% of the total inorganic sedimentation of medium silt if the marsh is 5 cm below mean high tide; this number rises 4.0% in 35 cm deep water. Calibrated values of suspended sediment concentration for coarse silt are 2.4 mg L^{-1} if flow depths are 5 cm during high tide and 0.88 mg L^{-1} if flow depths are 35 cm during high tide. Capture makes up a smaller percentage of the total sedimentation for coarse silt than for medium silt.

[33] Once the particle concentrations were calibrated to reproduce the measured accretion rate of 5.1 mm yr^{-1} in the unfertilized plots, simulations were run using the plant characteristics of the fertilized plots. Fertilized plots had greater biomass than unfertilized plots and also had different relationships between stem diameter and projected plant area per unit volume than the unfertilized plots: in fertilized plots, values for α and β were 0.078 and 0.68, respectively ($R^2 = 0.84$, $N = 255$) and values for μ and φ were 0.0013 and 0.20, respectively ($R^2 = 0.71$, $N = 1251$). Because the fertilized plots occupied a relatively small portion of the marsh (i.e., $< 1 \text{ m}^2$ plots), the water surface slope, calculated

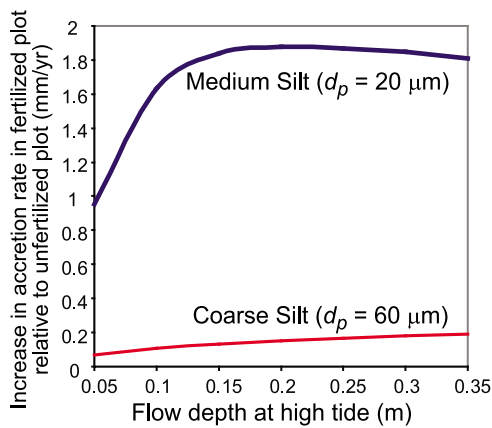


Figure 7. The increase in accretion rate of a fertilized plot on the Goat Island high marsh at North Inlet, South Carolina, relative to a nearby unfertilized control plot predicted by a model accounting for both particle capture and enhancements in particle settling brought about by a reduction in turbulent kinetic energy. Increase in accretion rate measured by *Morris et al.* [2002] was 2 mm yr^{-1} .

using equation (18), is assumed to be the same in fertilized and unfertilized plots. The drag coefficient and water surface slope are then used to calculate the flow velocity and turbulent kinetic energy on the fertilized plot.

[34] Enhancement of sedimentation due to the presence of plants can occur through three mechanisms. *Morris and Bradley* [1999] found that organic sedimentation could not account for the increase in total accretion of the fertilized plots. An increase in accretion could also occur due to enhanced particle capture or reduced turbulent energy resulting in increased effective settling velocities. Our calculations predict that particle capture will either not change (for flow depths of 0.35 m) or decrease (for flow depths of 0.05 m) in the fertilized plots. Two factors account for this decrease: (1) individual fertilized plants tend to grow larger but these larger plants reduce the stem density in fertilized plots, this in turn reduces the effectiveness of fertilized plants in capturing sediment, and (2) the reduced velocity in the fertilized stand due to greater drag forces reduces the effectiveness of particle capture (see Figure 5). For medium silt, particle capture in fertilized plots is reduced to 0.06% of the total sedimentation for maximum flow depths of 5 cm and 0.7% for maximum flow depths of 35 cm. Because of the strong reduction in particle capture efficiency within the fertilized plots due to a reduction in flow velocity, the rate of particle capture in the fertilized plots is less than in the unfertilized control plots. In contrast, the reduced flow velocity in the fertilized plots leads to significantly higher effective settling velocities: we find total sedimentation is enhanced in the fertilized plots and this enhanced sedimentation can be almost entirely (>99%) attributed to enhanced particle settling rather than particle capture.

[35] The total predicted increase in accretion rates in the fertilized plots due to particle capture and enhanced settling are shown in Figure 7. Predicted increases in accretion rate in fertilized relative to unfertilized plots can be as high as 1.9 mm yr^{-1} if the suspended sediment is primarily medium silt. The measured increase in the accretion rate

was 2.0 mm yr^{-1} [*Morris et al.*, 2002]. These model predictions should be considered approximations due to the uncertainties in flow velocities and flooding depths on the marsh surface. We emphasize, however, that flow velocities are within the range of those measured at nearby sites, modern sediments at nearby sites are made up of medium silt, and the only tuned parameter is the suspended concentration needed to achieve the background sedimentation rate. In summary, over the known range of values for particle size and flow velocity, the increased sedimentation measured by *Morris et al.* [2002] can only be explained through enhanced settling as a result of a reduction of turbulent kinetic energy on the fertilized plot, and the best estimates of these parameters produce a predicted increase in accretion rate that is within 5% of the measured increase.

7. Controls on Biologically Mediated Sedimentation

[36] Equations (8)–(19) may be used to investigate how inorganic sedimentation rates on marsh surfaces change as a function of flow depth, flow velocity, biomass, particle diameter, and suspended sediment concentration. Individual marshes will have unique vegetation characteristics (e.g., Figure 4), but here we explore the sensitivity of accretion rates at a point in a high marsh with vegetation characteristics similar to the Goat Island high marsh. In this analysis, we vary local parameter values (e.g., the velocity at a single point on the marsh). A spatially distributed study where particle sizes, concentrations, and other parameters vary as a function of distance from marsh creeks is beyond the scope of this study. Simulations are analogous to those in section 5 except the peak biomass is allowed to vary as a function of depth below mean high tide D [L] [e.g., *Morris et al.*, 2002],

$$\begin{aligned}
 B_p &= 0 & D < D_{\min} \\
 B_p &= \frac{B_{\max}}{D_{\max} - D_{\min}} (D - D_{\min}) & D_{\min} \leq D \leq D_{\max}, \\
 B_p &= 0 & D > D_{\max}
 \end{aligned} \quad (20)$$

where B_p [dimensions M L^{-2}] is the peak biomass, B_{\max} [M L^{-2}] is the biomass at the optimal depth below mean high tide, and D_{\min} and D_{\max} are the minimum and maximum depths below mean high tide that define the limits of macrophyte survival.

[37] Following *McKee and Patrick* [1988] and *Kirwan and Guntenspergen* [2010], we calculate D_{\max} as a function of tidal range T_r ,

$$D_{\max} = 0.7167 \times T_r - 0.483. \quad (21)$$

[38] The parameters B_{\max} and D_{\min} are set to 2500 g m^{-2} and 0 m, respectively, and the density of the marsh sediment is assumed to be 800 kg m^{-3} . Modeled accretion rates are linearly proportional to the inverse of marsh sediment density. The maximum biomass and minimum depth are based on data from North Inlet, but similar values can be found in other Atlantic and Gulf coast marshes. These values, however, are approximations and serve only to allow a study of

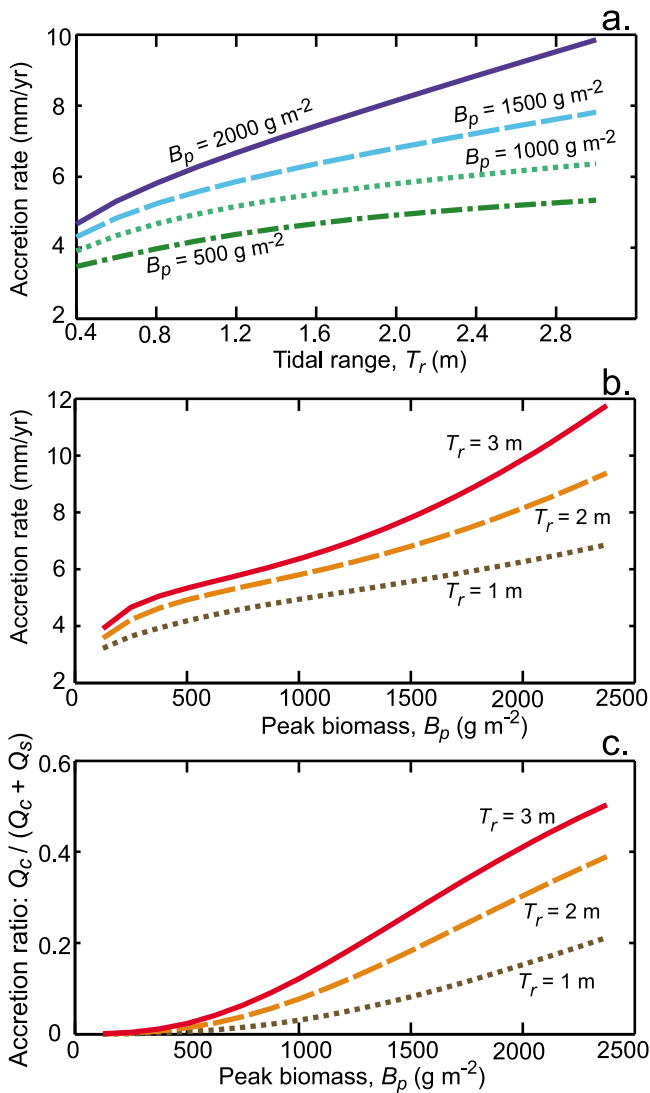


Figure 8. (a, b) Accretion rates and (c) accretion ratios ($Q_c / Q_T = Q_c / (Q_c + Q_s)$) as a function of peak biomass and tidal range. Other parameters held constant: peak flow velocity = 0.1 m s^{-1} , particle concentration = 20 mg L^{-1} , and particle diameter = $20 \text{ }\mu\text{m}$.

the sensitivity of the model to parameter values rather than provide exact predictions.

[39] The accretion rate due to capture and settling are linearly related to particle concentrations (see equations (8) and (9)). In Figures 8 and 9, the “accretion rate” is the total accretion rate from capture and settling: erosion, organic accretion, and compaction are neglected. Accretion rates are less than linearly related to tidal range, i.e., accretion rates increase with tidal range but the rate of increase is reduced for greater tidal range (Figure 8a). Tidal range, flow depth, and peak biomass are all related through equations (20) and (21). In Figure 8b, we plot accretion rates as a function of peak biomass (biomass varies throughout the year, the peak biomass is the maximum biomass attained during the summer). At low biomass (corresponding to shallow flows, see equation (20)), accretion rates are less than linearly related to peak biomass. As biomass increases, accretion rates

increase more rapidly as a function of biomass. This is because at high peak biomass values, particle capture becomes efficient due to greater leaf areas, occasionally exceeding 30% of the total accretion rate (Figure 8c).

[40] Accretion rates are, for the most part, inversely proportional to flow velocity (Figure 9a). The only exception to this general trend is when flow depths are great (i.e., approaching D_{max}) and particle capture makes up a large fraction of the total accretion rate (not shown). Inorganic accretion in typical marshes will be dominated by settling (see section 4), so any increase in particle capture due to increased flow velocity is offset by reduced settling that results from greater turbulent kinetic energy in faster flows. This increase in turbulent kinetic energy and the concomitant decrease in particle settling velocity accounts for the sharp decline in accretion rates as flow velocities increase. Accretion rates are most sensitive to changes in the diameter of the particles in suspension (Figure 9b). If particle diameters increase from medium silt to fine sand, one can expect large increases in accretion rates, all else equal. Again, these results are for a fixed flow depth. Were the marsh surface allowed to evolve, the high accretion rates for fine sands shown in Figure 9b would result in rapid upward growth of the marsh surface until the rate of accretion matched the rate of relative sea level rise. Thus, one would

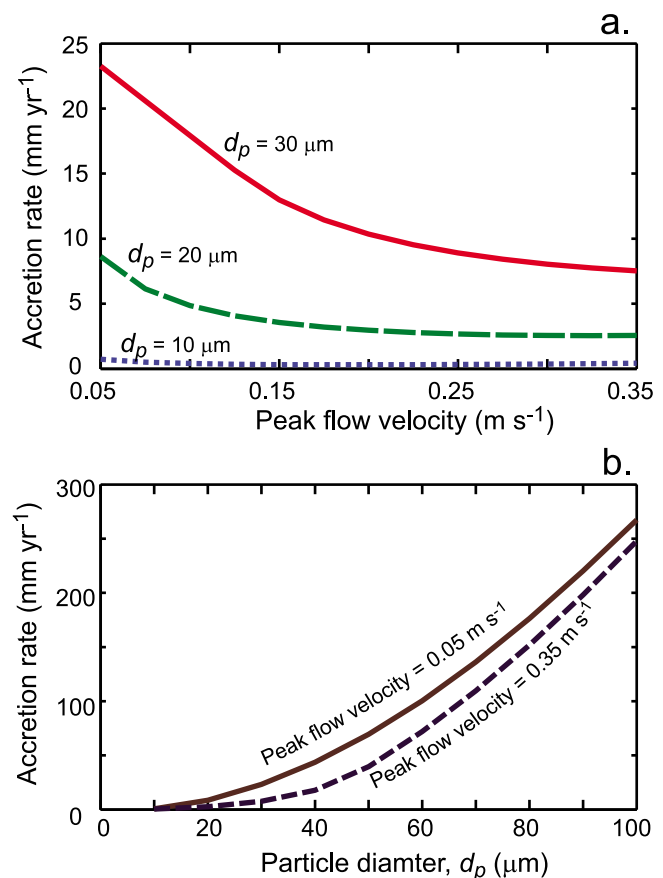


Figure 9. Accretion rates as a function of (a) peak flow velocity and (b) particle diameter. Other parameters held constant: peak biomass = 625 g m^{-2} , particle concentration = 20 mg L^{-1} , and tidal range = 1.5 m .

expect marshes with fine sands to sit high in the tidal frame relative to marshes composed of fine silt.

8. Conclusions

[41] By combining results from previously reported laboratory experiments with an extensive, 18 year data set of the physical characteristics of salt marsh macrophytes, we have been able to quantify the rate sediment is captured directly on plant stems within *Spartina alterniflora* marsh canopies and the biologically mediated settling velocity of particles delivered to the marsh during tidally induced floods. Comparing our extensive data set with similar data reported for other marsh species and locations, we find that the projected plant areas per unit volume and stem diameters reported here for *Spartina alterniflora* are broadly similar to those of other species in other locations, although we find that the macrophytes at the site of our measurements, the North Inlet estuary in South Carolina, USA, are likely to have high particle capture rates compared with other reported field sites. We find that particle capture is strongly dependent on marsh flow velocities, and at extreme flow velocities ($>0.4 \text{ m s}^{-1}$) particle capture can account for over 70% of the sediment delivered to the marsh from tidally induced flood waters. In typical marshes, however (flow velocities $<0.1 \text{ m s}^{-1}$), particle capture is expected to make up less than 10% of the sediment delivered from flood waters.

[42] A previously reported fertilization experiment at North Inlet found that accretion increased significantly after fertilization and that this increased sedimentation was derived from flood waters and not direct organic deposition [Morris *et al.*, 2002]. Here we discover that the particle capture mechanism cannot explain this added sediment. An increase in biomass on the marsh does however reduce the turbulent kinetic energy over the marsh surface, and this reduction in turbulent kinetic energy serves to increase the effective settling velocity of particles in suspension. By explicitly modeling particle capture and turbulent kinetic energy on fertilized and unfertilized marshes, we predict the magnitude of increased sedimentation due to increased biomass within the fertilized plots. The model is calibrated by tuning the suspended sediment concentrations so that the predicted accretion rate of the unfertilized plots matches the measured accretion rate. No other parameters are tuned. We find that if the suspended sediment is $20 \mu\text{m}$ in diameter (the particle size of modern sediments at the site reported by Gardner and Porter [2001]) the predicted increase in accretion rate is $\sim 1.9 \text{ mm yr}^{-1}$; Morris *et al.* [2002] measured an increase of 2.0 mm yr^{-1} of accretion in the fertilized plots relative to the unfertilized plots.

Notation

- a_c projected plant area per unit volume [L^{-1}].
- α_k coefficient relating kinetic energy to drag [dimensionless].
- α_0, α_1 coefficients for determining drag [dimensionless].
- α empirical coefficient relating biomass to projected plant area.
- A dimensionless empirical coefficient used for calculating settling velocity.

- β empirical coefficient relating biomass to projected plant area.
- B biomass per unit area of marsh macrophytes [M L^{-2}].
- B_p peak biomass [M L^{-2}].
- B_{max} biomass at the optimal depth below mean high tide [M L^{-2}].
- C_D depth averaged drag coefficient within the array of cylinders [dimensionless].
- C concentration of suspended sediment [M L^{-3}].
- C_{mp} rate of compaction [L T^{-1}].
- χ, ζ empirical coefficients relating drag to stems [dimensionless].
- d_c diameter of the collector (the stem diameter) [L].
- d_p particle diameter [L].
- $D_{\text{min}}, D_{\text{max}}$ minimum and maximum depths below mean high tide that define the limits of macrophyte survival, respectively [L].
- E erosion rate [L T^{-1}].
- η dimensionless particle capture efficiency.
- F dimensionless empirical coefficient used for calculating settling velocity.
- g acceleration due to gravity [L T^{-2}].
- γ dimensionless empirical coefficient for calculating particle capture efficiency.
- h flow depth [L].
- κ_{vk} von Karman's constant [dimensionless].
- κ dimensionless empirical coefficient for calculating particle capture efficiency.
- k turbulent energy per unit mass of water [$\text{L}^2 \text{T}^{-2}$].
- l_c total length of the collector (i.e., total length of stems within a control volume) [L].
- m dimensionless empirical coefficient used for calculating settling velocity.
- μ empirical coefficient relating biomass to stem diameter.
- n_c number of stems per unit area.
- ν kinematic viscosity of water [$\text{L}^2 \text{T}^{-1}$].
- O organic accretion rate [L T^{-1}].
- ω constant of proportionality relating shear stress to turbulent kinetic energy [dimensionless].
- ϕ empirical coefficient relating biomass to stem diameter.
- P number of particles per unit volume of water.
- Q_c rate of mass captured directly captured by plants stems per unit area of the marsh [$\text{M L}^{-2} \text{T}^{-1}$].
- Q_c rate of mass that settles out of suspension onto the surface of the marsh [$\text{M}^2 \text{T}^{-1}$].
- Re_c Reynolds number based on the collector diameter [dimensionless].
- R ratio of particle diameter to collector diameter [dimensionless].
- ρ_w density of water [M L^{-3}].
- ρ_s density of the marsh sediments [M L^{-3}].
- s ratio between the particle density and the density of water [dimensionless].
- S water surface slope [dimensionless].
- σ dimensionless empirical coefficient for calculating particle capture efficiency.
- τ shear stress [$\text{M L}^{-1} \text{T}^{-1}$].
- T_r tidal range [L].

- u flow velocity [$L T^{-1}$].
 u_* shear velocity [$L T^{-1}$].
 w_{eff} effective settling velocity of the particles in suspension [$L T^{-1}$].
 w_s settling velocity in turbulence-free water [$L T^{-1}$].
 w_{up} minus any component of upward velocity of particles in suspension caused by turbulence [$L T^{-1}$].
 V volume of water flowing through the marsh macrophytes [L^3].
 ζ_s elevation of the marsh surface [dimensions L].

[43] **Acknowledgments.** We thank the associate editor, two anonymous reviewers, and Brad Murray for their helpful comments. This work was supported in part by NSF grants DEB-0316429 and OCE-0423565.

References

- Allen, J. R. L. (1994), A continuity-based sedimentological model for temperate-zone tidal salt marshes, *J. Geol. Soc. London*, *151*, 41–49.
- Amos, C. L., A. Bergamasco, G. Umgiesser, S. Cappucci, D. Cloutier, L. DeNat, M. Flindt, M. Bonardi, and S. Cristante (2004), The stability of tidal flats in Venice lagoon – The results of in situ measurements using two benthic, annular flumes, *J. Mar. Syst.*, *51*, 211–241.
- Bradley, P. M., and J. T. Morris (1990), Physical characteristics of salt-marsh sediments – Ecological implications, *Mar. Ecol. Prog. Ser.*, *61*, 245–252.
- Camenen, B. (2007), Simple and general formula for the settling velocity of particles, *J. Hydraul. Eng. ASCE*, *133*, 229–233, doi:10.1061/(ASCE)0733-9429(2007)133:2(229).
- Chmura, G. L., S. C. Anisfeld, D. R. Cahoon, and J. C. Lynch (2003), Global carbon sequestration in tidal, saline wetland soils, *Global Biogeochem. Cycles*, *17*(4), 1111, doi:10.1029/2002GB001917.
- Christiansen, T., P. L. Wiberg, and T. G. Milligan (2000), Flow and sediment transport on a tidal salt marsh surface, *Estuarine Coastal Shelf Sci.*, *50*, 315–331.
- D’Alpaos, A., S. Lanzoni, S. M. Mudd, and S. Fagherazzi (2006), Modeling the influence of hydroperiod and vegetation on the cross-sectional formation of tidal channels, *Estuarine Coastal Shelf Sci.*, *69*, 311–324.
- D’Alpaos, A., S. Lanzoni, M. Marani, and A. Rinaldo (2007), Landscape evolution in tidal embayments: Modeling the interplay of erosion, sedimentation, and vegetation dynamics, *J. Geophys. Res.*, *112*, F01008, doi:10.1029/2006JF000537.
- Dietrich, W. E. (1982), Settling Velocity of Natural Particles, *Water Resour. Res.*, *18*, 1615–1626, doi:10.1029/WR018i006p01615.
- Fagherazzi, S., L. Carniello, L. D’Alpaos, and A. Defina (2006), Critical bifurcation of shallow microtidal landforms in tidal flats and salt marshes, *Proc. Natl. Acad. Sci. USA*, *103*, 8337–8341.
- French, J. R. (1993), Numerical-Simulation of Vertical Marsh Growth and Adjustment to Accelerated Sea-Level Rise, North Norfolk, UK, *Earth Surf. Processes Landforms*, *18*, 63–81.
- French, J. R., and D. R. Stoddart (1992), Hydrodynamics of salt-marsh creek systems – implications for marsh morphological development and material exchange, *Earth Surf. Processes Landforms*, *17*, 235–252.
- Gardner, L. R., and D. E. Porter (2001), Stratigraphy and geologic history of a southeastern salt marsh basin, North Inlet, South Carolina, USA, *Wetlands Ecol. Manage.*, *9*, 371–385.
- Gardner, L. R., B. Kjerfve, and D. M. Petrecca (2006), Tidal fluxes of dissolved oxygen at the North Inlet-Winyah Bay National Estuarine Research Reserve, *Estuarine Coastal Shelf Sci.*, *67*, 450–460.
- Gleason, M. L., D. A. Elmer, N. C. Pien, and J. S. Fisher (1979), Effects of stem density upon sediment retention by salt-marsh cord grass, *Spartina alterniflora* Loisel, *Estuaries*, *2*, 271–273.
- Hopkinson, C. S., J. G. Gosselink, and R. T. Parrondo (1980), Production of coastal Louisiana marsh plants calculated from phenometric techniques, *Ecology*, *61*, 1091–1098.
- Kim, S. C., C. T. Friedrichs, J. P. Y. Maa, and L. D. Wright (2000), Estimating bottom stress in tidal boundary layer from acoustic Doppler velocimeter data, *J. Hydraul. Eng. ASCE*, *126*, 399–406.
- Kirwan, M. L., and G. R. Guntenspergen (2010), Influence of tidal range on the stability of coastal marshland, *J. Geophys. Res.*, *115*, F02009, doi:10.1029/2009JF001400.
- Kirwan, M. L., and A. B. Murray (2007), A coupled geomorphic and ecological model of tidal marsh evolution, *Proc. Natl. Acad. Sci. U. S. A.*, *104*, 6118–6122.
- Kirwan, M. L., and S. Temmerman (2009), Coastal marsh response to historical and future sea-level acceleration, *Quat. Sci. Rev.*, *28*, 1801–1808, doi:10.1016/j.quascirev.2009.02.022.
- Kirwan, M. L., G. R. Guntenspergen, and J. T. Morris (2009), Latitudinal trends in *Spartina alterniflora* productivity and the response of coastal marshes to global change, *Global Change Biol.*, *15*, 1982–1989.
- Krone, R. B. (1987), A method for simulating historic marsh elevations, in *Coastal Sediments ’87*, edited by N. C. Krause, pp. 316–323, American Society of Civil Engineers, New York.
- Leonard, L. A., and A. L. Croft (2006), The effect of standing biomass on flow velocity and turbulence in *Spartina alterniflora* canopies, *Estuarine Coastal Shelf Sci.*, *69*, 325–336.
- Leonard, L. A., and M. E. Luther (1995), Flow hydrodynamics in tidal marsh canopies, *Limnol. Oceanogr.*, *40*, 1474–1484.
- Li, H., and S. L. Yang (2009), Trapping effect of tidal marsh vegetation on suspended sediment, Yangtze Delta, *J. Coast. Res.*, *25*, 915–936.
- Lightbody, A. F., and H. M. Nepf (2006), Prediction of velocity profiles and longitudinal dispersion in emergent salt marsh vegetation, *Limnol. Oceanogr.*, *51*, 218–228.
- Marani, M., A. D’Alpaos, S. Lanzoni, L. Carniello, and A. Rinaldo (2007), Biologically-controlled multiple equilibria of tidal landforms and the fate of the Venice lagoon, *Geophys. Res. Lett.*, *34*, L11402, doi:10.1029/2007GL030178.
- McKee, K. L., and W. H. Patrick (1988), The relationship of smooth cordgrass (*Spartina alterniflora*) to tidal datums – a review, *Estuaries*, *11*, 143–151.
- Morris, J. T. (1989), Modeling light-distribution within the canopy of the marsh grass *Spartina alterniflora* as a function of canopy biomass and solar angle, *Agr. Forest Meteorol.*, *46*, 349–361.
- Morris, J. T., and B. Haskin (1990), A 5-yr record of aerial primary production and stand characteristics of *Spartina alterniflora*, *Ecology*, *7*, 2209–2217.
- Morris, J. T., and P. M. Bradley (1999), Effects of nutrient loading on the carbon balance of coastal wetland sediments, *Limnol. Oceanogr.*, *44*, 699–702.
- Morris, J. T., P. V. Sundareswarar, C. T. Nietch, B. Kjerfve, and D. R. Cahoon (2002), Responses of coastal wetlands to rising sea level, *Ecology*, *83*(10), 2869–2877.
- Morris, J. T., et al. (2005), Integrating LIDAR elevation data, multi-spectral imagery and neural network modeling for marsh characterization, *Int. J. Remote Sens.*, *26*, 5221–5234.
- Mudd, S. M., S. Fagherazzi, J. T. Morris, and D. J. Furbish (2004), Flow, sedimentation, and biomass production on a vegetated salt marsh in South Carolina: Toward a predictive model of marsh morphologic and ecologic evolution, in *The Ecogeomorphology of Tidal Marshes, Coastal Estuarine Monogr. Ser.*, edited by S. Fagherazzi, A. Marani, and L. K. Blum, pp. 165–187, American Geophysical Union, Washington, D. C.
- Mudd, S. M., S. M. Howell, and J. T. Morris (2009), Impact of dynamic feedbacks between sedimentation, sea level rise, and biomass production on near surface marsh stratigraphy and carbon accumulation, *Estuarine Coastal Shelf Sci.*, *82*, 377–389, doi:10.1016/j.ecss.2009.01.028.
- Nepf, H. M. (1999), Drag, turbulence, and diffusion in flow through emergent vegetation, *Water Resour. Res.*, *35*, 479–489, doi:10.1029/1998WR000069.
- Netto, S. A., and P. C. Lana (1997), Influence of *Spartina alterniflora* on superficial sediment characteristics of tidal flats in Paranaguá Bay (South-Eastern Brazil), *Estuarine Coastal Shelf Sci.*, *44*, 641–648.
- Neubauer, S. C. (2008), Contributions of mineral and organic components to tidal freshwater marsh accretion, *Estuarine Coastal Shelf Sci.*, *78*, 78–88.
- Neumeier, U., and P. Ciavola (2004), Flow resistance and associated sedimentary processes in a *Spartina maritima* salt-marsh, *J. Coastal Res.*, *20*, 435–447.
- Nyman, J. A., R. J. Walters, R. D. Delaune, and W. H. Patrick (2006), Marsh vertical accretion via vegetative growth, *Estuarine Coastal Shelf Sci.*, *69*, 370–380.
- Orson, R., W. Panagiotou, and S. P. Leatherman (1985), Response of tidal salt marshes of the United States Atlantic and Gulf Coasts to rising sea levels, *J. Coastal Res.*, *1*, 29–37.
- Orton, P. M., and G. C. Kineke (2001), Comparing calculated and observed vertical suspended-sediment distributions from a Hudson River Estuary turbidity maximum, *Estuarine Coastal Shelf Sci.*, *52*(3), 401–410.
- Palmer, M. R., H. M. Nepf, and T. J. R. Pettersson (2004), Observations of particle capture on a cylindrical collector: Implications for particle accumulation and removal in aquatic systems, *Limnol. Oceanogr.*, *49*, 76–85.
- Pezeshki, S. R., and R. D. DeLaune (1988), Carbon assimilation in contrasting streamside and inland *Spartina alterniflora* salt-marsh, *Vegetatio*, *76*, 55–61.

- Ranwell, D. S. (1964), *Spartina* salt marshes in Southern England: 2. Rate and seasonal pattern of sediment accretion, *J. Ecol.*, *52*, 79–94.
- Redfield, A. C. (1972), Development of a New England Salt Marsh, *Ecol. Monogr.*, *42*, 201–237.
- Shi, Z., L. J. Hamilton, and E. Wolanski (2000), Near-bed currents and suspended sediment transport in saltmarsh canopies, *J. Coastal Res.*, *16*, 909–914.
- Shimeta, J., and P. A. Jumars (1991), Physical-mechanisms and rates of particle capture by suspension-feeders, *Oceanogr. Mar. Biol.*, *29*, 191–257.
- Soulsby, R. L., and K. R. Dyer (1981), The form of the near-bed velocity profile in a tidally accelerating flow, *J. Geophys. Res.*, *86*, 8067–8074, doi:10.1029/JC086iC09p08067.
- Stapleton, K. R., and D. A. Huntley (1995), Seabed stress determinations using the inertial dissipation method and the turbulent kinetic energy method, *Earth Surf. Processes Landforms*, *20*, 807–815.
- Stumpf, R. P. (1983), The process of sedimentation on the surface of a salt-marsh, *Estuarine Coastal Shelf Sci.*, *17*, 495–508.
- Tanino, Y., and H. M. Nepf (2008), Laboratory investigation on mean drag in a random array of rigid, emergent cylinders, *J. Hydraul. Eng. ASCE*, *134*, 34–41, doi:10.1061/(ASCE)0733-9429(2008)134:1061(1034).
- Temmerman, S., G. Govers, P. Meire, and S. Wartel (2003), Modelling long-term tidal marsh growth under changing tidal conditions and suspended sediment concentrations, Scheldt estuary, Belgium, *Mar. Geol.*, *193*(1–2), 151–169.
- Temmerman, S., et al. (2005), Impact of vegetation on flow routing and sedimentation patterns: Three-dimensional modeling for a tidal marsh, *J. Geophys. Res.*, *110*, F04019, doi:10.1029/2005JF000301.
- Torres, R., and R. Styles (2007), Effects of topographic structure on salt marsh currents, *J. Geophys. Res.*, *112*, F02023, doi:10.1029/2006JF000508.
- Valiela, I., J. M. Teal, and W. G. Deuser (1978), Nature of growth forms in salt-marsh grass *Spartina alterniflora*, *Am. Nat.*, *112*, 461–470.
- Yang, S. L. (1998), The role of scirpus marsh in attenuation of hydrodynamics and retention of fine sediment in the Yangtze Estuary, *Estuarine Coastal Shelf Sci.*, *47*, 227–233.
- Yang, S. L., H. Li, T. Ysebaert, T. J. Bouma, W. X. Zhang, Y. Y. Wang, P. Li, M. Li, and P. X. Ding (2008), Spatial and temporal variations in sediment grain size in tidal wetlands, Yangtze Delta: On the role of physical and biotic controls, *Estuarine Coastal Shelf Sci.*, *77*, 657–671.

A. D'Alpaos, Department of Geosciences, University of Padova, Via Giotto, 1, Padova, PD I-35137, Italy. (andrea.dalpaos@unipd.it)

J. T. Morris, Belle W. Baruch Institute for Marine and Coastal Sciences, University of South Carolina, Columbia, SC 29208, USA. (morris@biol.sc.edu)

S. M. Mudd, School of GeoSciences, University of Edinburgh, Edinburgh EH8 9XP, UK. (simon.m.mudd@ed.ac.uk)